CROATICA CHEMICA ACTA CCACAA 63 (3) 331—353 (1990)

CCA-1944

YU ISSN 0011-1643
UDC 541.183
Conference Paper (Invited)

Disordered Solid Surfaces: Characterization and Properties*

Klaus Wandelt

Institut für Physikalische und Theoretische Chemie, Universität Bonn, Wegelerstr. 12, 5300 Bonn 1, F. R. G.

Received May 10, 1990

Atomic scale surface disorder (defects) has an important — if not dominating — influence on the physical and chemical properties of solid surfaces, e. g. on their reactive and catalytic behavior. This holds certainly for both solid/gas and solid/liquid interfaces. In this work a technique is described, Photoemission of Adsorbed Xenon (PAX), which enables a surface characterization on the atomic scale under ultrahigh vacuum conditions. The information obtained, namely the relative concentration of chemical and structural defects as well as local surface potential differences and local fields arising from them, appears equally important for an understanding of solid/gas and solid/liquid interfaces.

1. INTRODUCTION

There exists abundant evidence that the physical as well as the chemical properties of surfaces are strongly effected — if not dominated — by surface defects, that is atomic scale disorder. It is well established, that the sticking coefficient of gases is influenced by structure defects at surfaces (e. g. 1). Already small amounts of copper on a ruthenium surface inhibit hydrogen adsorption[2]. By contrast, adsorbed alkali metals enhance the reactivity of metal[3] or semiconductor surfaces (promotion)[4]. The pioneering work by Somorjai[5] with well defined vicinal surfaces clearly demonstrated the influence of step- and kink-defects on the selectivity of the C-C- and C-H-rupture of hydrocarbons. Defects govern the nucleation and growth processes in epitaxial film and crystal growth. From these examples it becomes clear that a full understanding of the physical and chemical surface properties requires the characterization of surfaces on the atomic scale, in order to be able to consider their heterogeneity. This insight has led to the development of new experimental techniques which are able to provide this atomic scale information, such as (above all) the scanning tunneling microscope (STM) /e. g. 6/, the low energy electron reflection/diffraction microscope (LEEM)[7] and the photoelectron spectroscopy of adsorbed xenon (PAX)[8], to name only some.

Figure 1 shows a Kossel model of a more or less realistic surface which contains structural defects such as steps, kinks, ad-atoms and vacancies as

* Based on an invited lecture presented at the *8th „Ruđer Bošković" Institute's International Summer Conference on the Chemistry of Solid/Liquid Interfaces* Red Island, Rovinj, Croatia, Yugoslavia, June 22 — July 1, 1989.

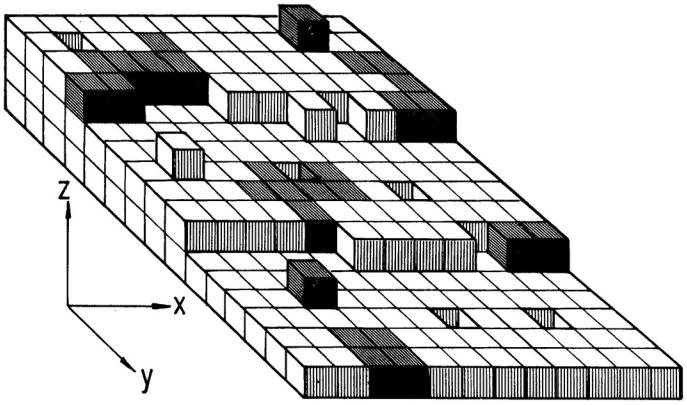

Figure 1. Kossel model of a realistic surface.

well as two atomic constituents (dark and white). As a consequence the properties of this surface, in particular, the electron density and thereby the electrostatic surface potential varies within the surface plane (x, y). The only reasonable way to understand such complex surfaces appears to be the use of model surfaces which are prepared to contain first predominantly one kind of defect only. In the next step two kinds of defects may be combined, etc. The present contribution describes the capability of the PAX-technique to characterize this kind of atomic-scale surface disorder and to enable a correlation of the properties of particular surface defects with the macroscopic physical and chemical properties of such surfaces. The PAX-technique will be described in detail in section 2.; at places brief comparison with STM will be made. While the STM is an imaging technique which provides real space images from the atomic structure of surfaces, the PAX-technique is a kind of decoration method which enables the titration of specific surface sites and which, in particular, provides a tool to determine local surface potential variations. Various examples will be presented to demonstrate the capability of the PAX-technique[8] and the studies will include a) the characterization of step-defects as well as their influence on the adsorption of molecules (section 3), b) the study of metal adsorbates on metal and semiconductor substrates (section 4), and c) the growth and stability of submonolayer and bilayer alloy films (section 5). The main conclusions are summarized in section 6.

2. THE PAX-TECHNIQUE

Below $\sim$ 80 K the rare gas xenon can be »physisorbed« on any solid surface. The UV (HeI) excited photoemission spectrum of Xe adsorbed on a Ru(001) surface is displayed in Figure 2. The two sharp extra peaks (above the Ru background, dashed line) between 5 and 7 eV below E_F arise from the $5p_{3/2}$ and $5p_{1/2}$ photoemission final states of adsorbed Xe atoms. For the sake of clarity and ease we will concentrate on the $5p_{1/2}$ signal only, because its physical structure is somewhat simpler than that of the $5p_{3/2}$ signal[8], which becomes evident from Fig. 3. The $5p_{1/2}$-signal consists of only one Lorentzian line while the $5p_{3/2}$ consists of two Lorentzian lines, all three arising from the $5p_{1/2}$ ($m_j = \pm 1/2$), the $5p_{3/2}$ ($m_j = \pm 1/2$) and the $5p_{3/2}$ ($m_j = \pm 3/2$) final

states of photoionized Xe atoms, respectively. Due to the presence of the surface as well as of interactions between the adsorbed Xe atoms (twodimensional band structure formation) the two $5p_{3/2}$ final states are no longer degenerate as in the gas phase[9-13]. The important surface structural information will be retrieved from the $5p_{1/2}$ signal only, namely from its energy position, its intensity as well as its shape. But all the arguments and conclusions drawn hereof hold likewise for the $5p_{3/2}$ signal.

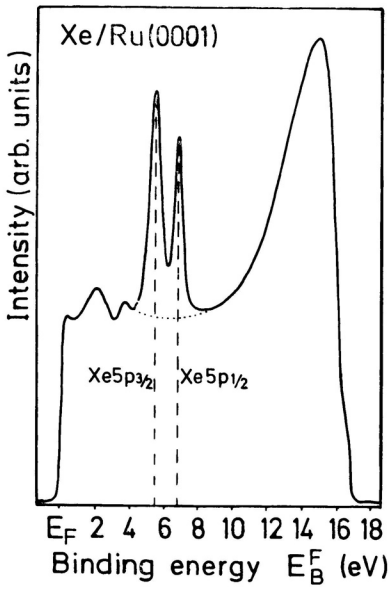

Figure 2. He(I) excited Xe ($5p_{3/2,1/2}$) photoemission spectrum from a Ru (001) surface covered with one complete monolayer of xenon.

In a number of publications (e. g. 8, 14—16) it has been shown, that the ionization potential of adsorbed Xe atoms (with respect to the vacuum level V) is rather independent of the substrat:

$$E_B^V(5p_{1/2}) = E_B^F(5p_{1/2}) + \varphi \approx \text{const.} \quad (1)$$

This correlation could, in fact, be verified by now for more than 25 single crystal substrates of quite different nature, including transition metals (Pd, Pt, Ir, Ni etc.), noble metals (Cu, Ag, Au), alkali metals (K, Cs), semiconductor surfaces (Si, ZnO) as well as oxides (TiO_2, ZnO). There are two physical reasons for this surprising invariance of $E_B^V(5p_{1/2})$. Firstly, the Xe — substrate interaction is very weak in all cases; typical Xe physisorption energies are smaller than $\sim$ 8 kcal/mol. As a consequence initial state bonding shifts, and in particular their changes between different substrates, are negligibly small (< 0.2 eV). Secondly, a Xe atom is rather big (diameter 4,5 Å). Therefore the center of an adsorbed Xe atom is located outside of the steeply varying electrostatic surface potential ϕ (Figure 4), which arises from the

surface dipole layer. As a consequence the potential well of an adsorbed Xe atom is »pinned« to the vacuum potential outside the surface dipole barrier and »floats« up and down when the work function φ of the substrate is chan-

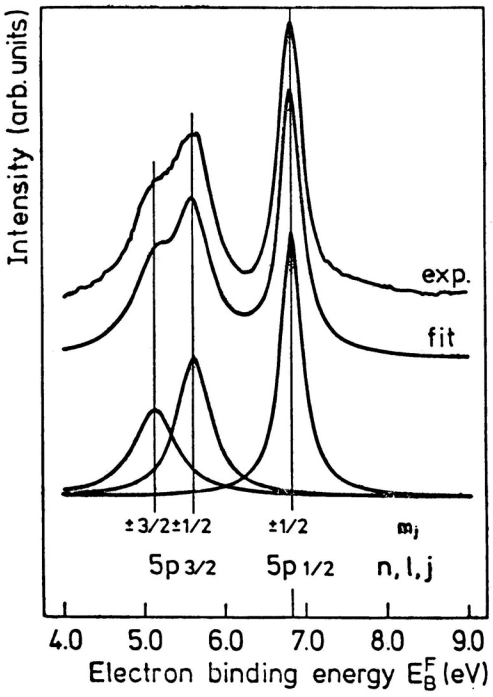

Figure 3. Experimental $5p_{3/2,1/2}$ UV-photoemission spectrum (exp) of one complete monolayer of Xenon adsorbed on an epitaxial monolayer of gold on Ru (001). The full line (fit) corresponds to the best fit with three Lorentzian functions representing the $5p_{3/2}$ ($m_j = \pm 3/2$), $5p_{3/2}$ ($m_j = \pm 1/2$) and $5p_{1/2}$ ($m_j = \pm 1/2$) final states of photoionized Xe; n, l, m_j = quantum numbers. The sharp Xe ($5p_{1/2}$) peak is best used for the distinction of different Xe adsorption sites.

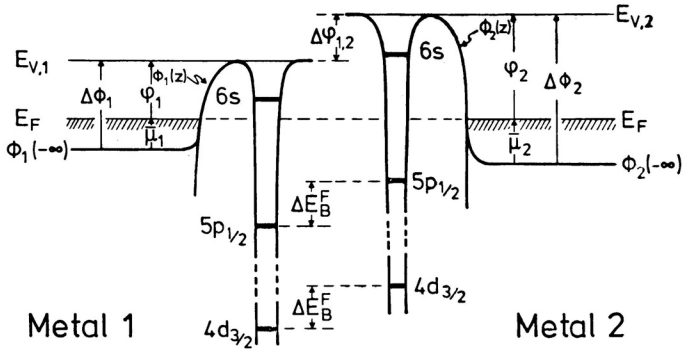

Figure 4. Energy level diagram for xenon adsorbed on two metals of different work function φ, illustrating the PAX mechanism based on equ. (1). (From Ref. 8b)

ged, for whatever reason, e. g. when changing the crystallographic orientation of the substrate surface, when changing the substrate material or when preadsorbing some other adsorbate. This »floating« model is illustrated in Figure 4 and has received strong theoretical[17] as well as experimental suppcrt. For instance, the same invariance as expressed in equ. (1) could be verified for the Xe (4d) and Xe (3d) core levels[18].

An immediate consequence of equ. (1) is:

$$\Delta E_B^F (5p_{1/2}) = -\Delta \varphi \tag{2}$$

as becomes clear from Figure 4. The important point is now, that this equation holds also for heterogeneous surfaces: Xe atoms being adsorbed on two »patches« of the same surface, which have different local work functions, differ in their E_B^F $(5p_{1/2})$ binding energy values (with respect to the Fermi level E_F) accordingly, and two Xe (5p) spectra appear simultaneously and shifted by

$$\Delta E_B^F (5p_{1/2}) = -\Delta \varphi_{local} \tag{3}$$

with respect to each other. This is illustrated in Figure 5. Equation (3) is the basis of PAX. Considering further, that the adsorption energy E_{ad} of Xe also

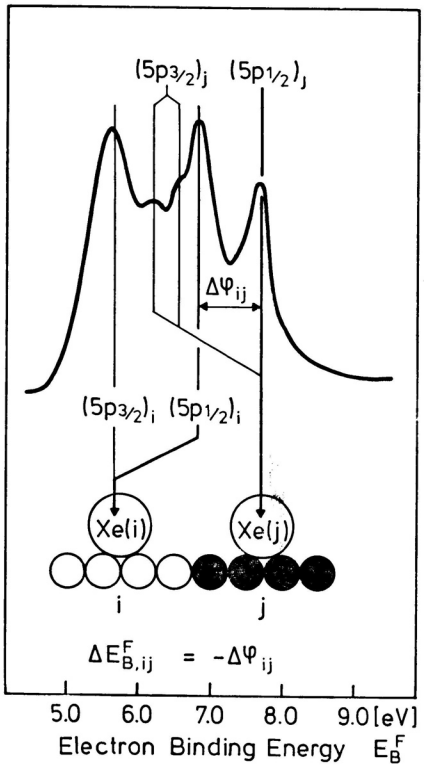

Figure 5. Superposition of $5p_{3/2,1/2}$ spectra of two coexisting Xe adsorption states on two kinds of surface patches i and j. The $(5p_{3/2})_i$ signal is only broadened, while the $(5p_{3/2})_j$ peak is split (see text). The shift $\Delta E_B^F (5p_{1/2})_{ij}$ is a measure of the local work function difference $\Delta \varphi_{ij}$ between both patches.

depends on the chemical nature and coordination of the specific adsorption site, different surface sites can be populated successively in the sequence of decreasing E_{ad} and can thus be characterized by PAX separately on an atomic scale[8,15,16,19]. The role of the adsorbed Xe atoms is nothing more than to deposit a »test electron« (bound e. g. in the 5p level) at a particular surface site (controlled by E_{ad}) which then via photoemission provides information about the surface potential at this site. Beyond the distinction of different kinds of surface sites by their $5p_{1/2}$ electron binding energy (qualitative analysis) evaluation of the corresponding partial intensities yields the surface concentration of each kind of site (quantitative analysis). The following sections present selected examples.

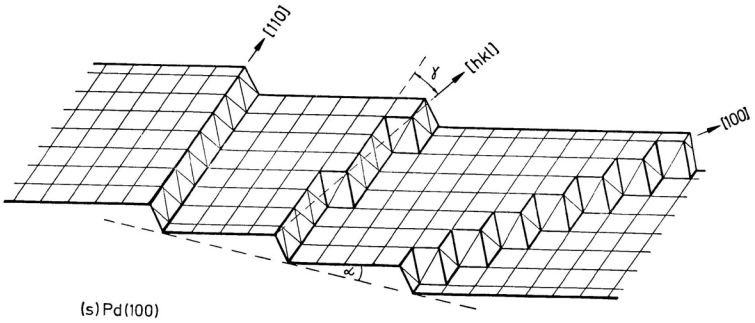

Figure 6. Schematic representation of stepped (s)Pd(100) vicinal surfaces with monoatomic steps of different orientation [hkl]. α = vicinal angle, γ = step direction off the [110] direction.

3. PROPERTIES AND INFLUENCE OF STEP DEFECTS

Steps and kinks are ubiquitous surface structure defects as has become clear from Scanning Tunneling Microscopy. The influence and the properties of these step defects at surfaces are studied best with well prepared vicinal surfaces as model systems[20], because they enable a control of the average step density and the crystallographic step direction. Vicinal surfaces are prepared by cutting a single crystal under a small angle ($\alpha < 10°$) off a low index crystal plane. After polishing and cleaning in ultrahigh vacuum such an equilibrated vicinal surface assumes a rather regular step structure which can be characterized very accurately by STM (e. g. 21) and LEED[20] with respect to the step height (which is mostly monoatomic), the crystallographic direction of the step ledges as well as the mean width W of the terraces between the steps. The terraces between two adjacent steps have the same structure as the parent low-index plane ($\alpha = 0°$), even if this surface tends to reconstruct.[21] Figure 6 shows schematically an fcc (100) surface with three monoatomic steps of different orientations [hkl]. Steps with [110] direction are formed from close-packed rows of atoms resulting in smooth ledges. Steps with directions γ off the [110] direction include kinks. In the [100] direction ($\gamma = 45°$) the step should be fully kinked.

Step wedges (including kinks) provide surface sites with high coordination to the substrate, and therefore physisorbed xenon atoms will preferably occupy (down-) step and kink sites before the terrace sites are populated[22].

This assumption is particularly justified in the case of physisorbed gases which are held at the surface by isotropic van der Waals forces.

Xe ($5p_{3/2,\ 1/2}$) UPS spectra from a stepped Pd (100) surface are displayed in Figure 7. It is clearly seen, that at low Xe coverages obtained after Xe exposures $<$ 4L Xe (spectra a-c) the $5p_{1/2}$ peak is located at somewhat higher electron binding energy than a second $5p_{1/2}$ peak which first becomes visible in spectrum d (4L) and which finally overgrows the low coverage signal. Spectrum g corresponds to a complete monolayer of Xe on this surface; its intensity serves as reference for the assignment of the lower coverages. A careful decomposition of the $5p_{1/2}$ intensity of the spectra from Figure 7 using three Lorentzian lines as shown in Figure 3 per Xe adsorption state yields two $5p_{1/2}$ lines which are separated by $\sim$ 350 meV. At Xe monolayer satura-

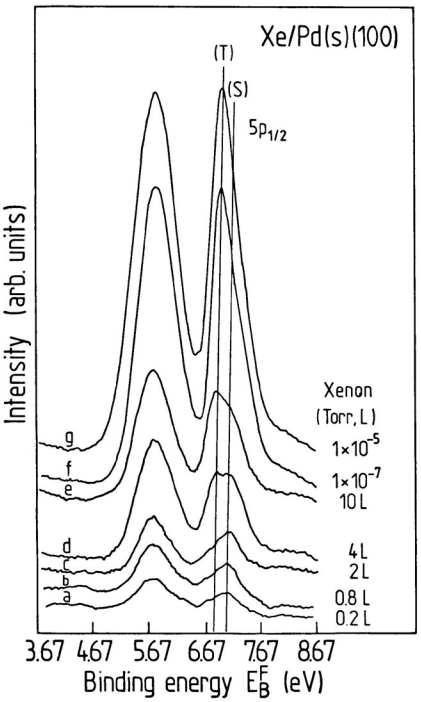

Figure 7. Xe ($5p_{3/2,1/2}$) spectra for Xe adsorption on a stepped Pd(100) vicinal surface. Note the sequential population of the step (s) and terrace sites (T) with xenon. The highest spectrum corresponds to a complete Xe monolayer on this surface. (From Ref. 25)

tion the intensities of both $5p_{1/2}$ peaks reflect the relative abundances of step- and terrace-sites on this surface which are known from a LEED-analysis. Of course, the initial selective population of the step sites clearly determines the assigment of the two $5p_{1/2}$ photoemission peaks seen in Figure 7, in that the higher binding energy peak (at low coverage) corresponds to Xe atoms at step sites [Xe (S)] and the lower binding energy peak to Xe atoms on terrace sites [Xe (T)]. Besides the energy shift of $E_B{}^F \approx 350$ meV between them, the

absolute $E_B^F(5p_{1/2}, S)$ value is very close to the value found on a perfect Pd (110) surface, namely 7,03 eV /23/. In turn, the E_B^F $(5p_{1/2}, T)$ value is near the value found on a perfect Pd (100) surface ($\alpha = 0°$ in Figure 6). Very similar results have been obtained with other Pd (100) vicinal surfaces of different step density and step orientation[24,25], and in all cases the experimentally determined intensity ratios $(Xe(T) : Xe(S))_{exp}$ agreed within $\sim 15\%$ with the $(Xe(T) : Xe(S))_{model}$ value estimated on the basis of an ideal terrace-ledge--kink model of the respective vicinal surface as derived from LEED and populated with hard-sphere Xe atoms.

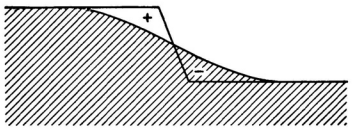

Figure 8. Schematic representation of the Smoluchowski electron smoothing effect near a surface step. Charge flows from the upper step edge into the low step wedge, thereby creating a localized extra dipole which counteracts the normal surface dipole layer.

Using equ. (3) the local surface potential at the step sites is $\Delta\varphi_{S,T} = \Delta E_B^F$ $(S,T) \approx 350$ meV lower than at the terrace sites. This is a consequence of the so-called Smoluchowski smoothing effect[26]. The electronic charge near the surface does not follow the abrupt step geometry but flows from the upper step edge into the lower step wedge (Figure 8). This creates a local extra dipole which is antiparallel to the normal surface dipole layer. Indeed, systematic studies with regularly stepped surfaces[24,27,28] revealed a linear decrease of the (macroscopic) work function of these surfaces as a function of step density. This linearity originally led to the indirect conclusion, that the step induced charge redistribution and, hence, the associated extra dipoles which counteract the normal surface dipole is really confined to the immediate vicinity of the steps. Each step adds an incremental dipole which leads to a linear decrease of the macroscopic work function with increasing step density. The present PAX results provide direct evidence that the surface potential is locally lowered by ~ 350 meV at a step site compared to a terrace site. Moreover, from the fact, that the $(Xe(T) : Xe(S))_{exp}$ intensity ratio determined at Xe monolayer saturation always agrees with the expectation based on the model derived numbers of available step and terrace sites, it follows conclusively that only those Xe atoms »feel« the lowered surface potential which are in immediate contact with the step; already the next nearest row of Xe atoms away from the step does not contribute to the Xe (S) signal. Consequently, PAX proves directly that the work function decrease is strictly localized along the steps. This, in turn, supports the notion, that the lateral »resolution« of the PAX technique is of the order of one Xe atom diameter, ~ 5 Å.

These observations make PAX an important tool for the characterization of surface steps. Of course, the »titration« of the number of step sites, and the local surface potential at a step site are basic quantities when it comes to an understanding of the physical and chemical properties of structurally defective surfaces. For instance, the local surface potential decrease at step

sites may be as large as $\sim$ 1eV measured at steps on a Pt (111) surface[29]. Since this potential difference decays over a distance of only a few Ångstroms the strong localized fields associated with these surface irregularities are expected to have strong influence on the properties of adsorbed molecules at these sites. These strong lateral fields have not been taken into account so far in order to explain the different reactivity of adsorbed molecules on heterogeneous surfaces, e. g. at step sites or near heteroatoms. A recent theoretical investigation of the effect of these lateral electric fields on e. g. the degenerate $2\pi^*$ derived valence levels of chemisorbed CO molecules[30] indicated, indeed, a strong (dominantly linear) dependence of level shifts and level broadening on the existing field. This feature, which can be considered as a local surface Stark effect, provides a mechanism which may be a clue to the understanding of some elementary processes in heterogeneous catalysis.

4. METAL ADSORBATES

4.1 Copper Adsorption on Ru(001)

PAX can also provide quantitative information about the concentration and lateral distribution of heteroatoms on a metal surface, as well as the electrostatic surface potential in their immediate vicinity.

Figure 9. shows a series of Xe ($5p_{3/2,1/2}$) spectra from a perfect Ru (001) surface, which prior to the Xe adsorption, was covered with $\sim$ 0.4 monolayers of copper by vapor deposition and well annealed at 520 K. Up to an exposure of 3 L Xe the spectra exhibit two $5p_{1/2}$ states at 6.75 eV and $\sim$ 7.1 eV, respectively. The dominant peak A at 6,75 eV is close to the position as on clean Ru, and is therefore assigned to Xe atoms on bare Ru patches; [Xe (Ru)]. Above 3 L Xe exposure a new $5p_{1/2}$ peak B emerges at $\sim$ 7.4 eV; its $5p_{3/2}$ counterpart grows between the $5p_{3/2}$ and $5p_{1/2}$ signals of the Xe (Ru) state. Signal B is very close to the position as on pure Cu (111) and is therefore assigned to Xe atoms on the deposited Cu; [Xe (Cu)]. The fact, that these Cu sites are populated with Xe after the Ru sites, is in agreement with the lower Xe adsorption energy on Cu compared to Ru[31,32]. The Xe (Cu) $5p_{3/2}$ signal (between the Xe (Ru) peaks) is clearly split into two peaks. It is generally accepted, that the origin of this splitting is the formation of a two-dimensional (2D) electronic band structure within the adsorbed Xe[12,13], which in the present case is only conceivable, if the Cu deposit forms flat islands so that the Xe atoms on top can also form a densely packed overlayer. Hence, the structure of the Xe (Cu) spectrum itself namely the $5p_{3/2}$ splitting, conveys the unambiguous information that submonolayers of Cu on Ru (001) form islands, which should be monoatomically thick, because the Cu-Ru interaction is stronger than the Cu-Cu interaction[33]. This together with the fact, that Cu and Ru are not miscible, and that therefore Cu forms 2D islands on the Ru surface leads to the assignment that the peak C in Figure 9 corresponds to Xe atoms at the (mixed) Cu/Ru step sites along the Cu island boundaries; [Xe/Cu/Ru)] (see inset of Figure 9). As has been demonstrated earlier with the similar Ag/Ru system[19] the partial intensities of all three Xe states, Xe (Ru), Xe (Cu) and Xe (Cu/Ru), are a quantitative measure of the relative abundances of these three kinds of surface sites, and the local surface potential at the mixed Cu/Ru boundary sites is intermediate between those on

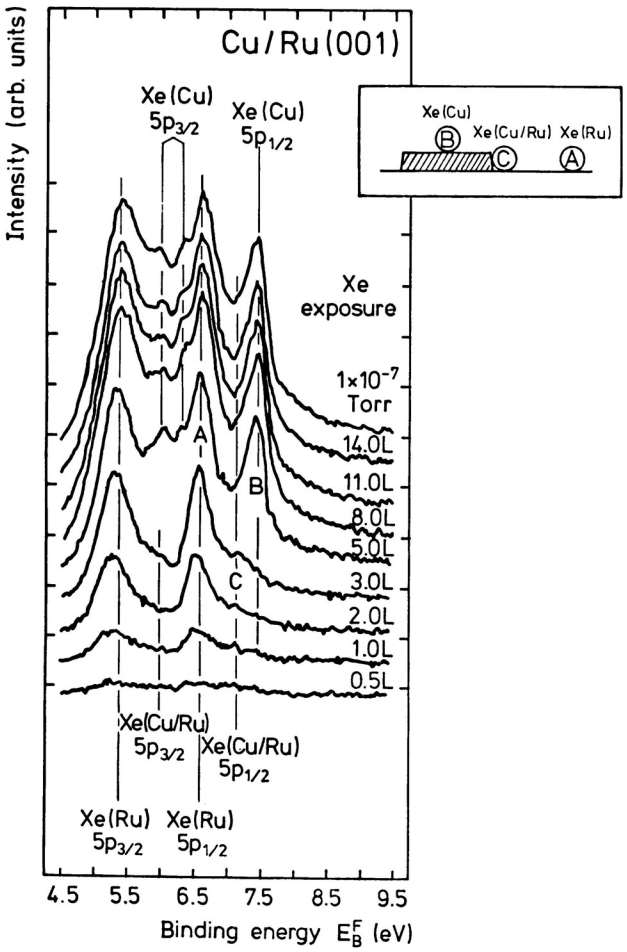

Figure 9. Xe ($5p_{3/2,1/2}$) spectra from a partly Cu-covered Ru(001) surface as a function of Xe coverage. Note the clear distinction of the emission peaks from Xe atoms on the three possible adsorption sites indicated in the inset. (From Ref. 51)

Ru and Cu patches, respectively. The assignment of peak C being due to Xe atoms at mixed Cu/Ru sites, by the way, is strongly supported by PAX spectra from a Cu covered Ru (001) surface, which prior to Cu deposition was slightly sputtered. In this case, formation of 2D Cu islands is prevented due to the high concentration of sputter-induced defect sites which act as heterogeneous nucleation centers[32].

This Cu/Ru example shows that PAX cannot only distinguish qualitatively between the three possible surface sites for Xe adsorption, namely Ru, Cu and Cu/Ru boundary sites, but also provides a quantitative measure of their relative surface concentration, their local surface potential by virtue of their $5p_{1/2}$ electron binding energies using equ. (3) as well as the distribu-

tion of the Cu deposit, namely 2D island formation on the flat Ru (001) substrate versus nearly atomic dispersion on a sputtered Ru substrate[32]. Even more spectacular PAX results could be obtained from a Ru (001) surface covered with 0.05 monolayers of potassium as described in the following.

4.2. *Potassium Adsorption on Ru(001) and Si(100)*

It is well established by many different experimental studies, that alkali metals adsorbed on both metal and semiconductor surfaces may reduce the work function by up to more than $\sim$ 4eV (e. g. 34) depending on the alkali metal substrate system and the adsorbate coverage. Typically at low coverage ($\Theta_{ALK} \leq 0.1$ ML) the work function decreases linearly with increasing alkali metal coverage. Around $\Theta_{ALK} \sim 0.5$ ML the work function change curve passes through a shallow minimum, and at monolayer completion ($\Theta_{ALK} = 1$ ML) the work function φ approaches already the value of the respective bulk alkali metal. This general behavior, which is not restricted to metal substrates, but has been observed for semiconductor surfaces likewise (e. g. Refs. 35, 36), is explained, since Langmuir[37-39], in terms of a strong, coverage dependent charge transfer from the alkali atoms to the substrate surface, because of the low ionization potential of alkali metals. As a result of this charge donation each adsorbed alkali atom leads to the creation of a dipole, the moment μ of which is antiparallel to that of the substrate surface dipole layer, thereby causing the observed work function decrease. At low alkali metal coverage the partially positive alkali ions repel each other electrostatically and it is safe to assume that individual ions are uniformly distributed across the surface. At these low coverages each ion donates the same amount of charge to the substrate as must be concluded from the linear initial decrease of the $\Delta\varphi(\Theta)$-curves. An important question concerns the spatial distribution of the negative extra charge which is donated to the substrate. Since this extra surface charge is expected to influence the surface potential of the substrate, locally resolved work function change measurements by means of PAX again appear to be an appropriate way to probe the range of the charge redistribution around individual alkali metal atoms adsorbed on a metal or semiconductor surface.

Figure 10 shows a model of the Ru (001) basal plane (white atoms) covered with 0.05 ML of potassium (black atoms) and with an overlayer of Xenon at 50 K (dotted atoms on Ru-atoms and big white atoms on K-atoms). This model is to illustrate two points which are important for the discussion of the experimental data shown below. Firstly, Xe atoms tend to form a hexagonally close-packed overlayer of monoatomic thickness nearly independent from the substrate structure. Secondly, five Xe atoms fit around one K-atom on the Ru (001) substrate. All three Xe-states, namely Xe on free Ru (001) sites [Xe (Ru)], Xe next to a K-atom [Xe (K/Ru)] and Xe ontop of a K-atom [Xe (K)], can be distinguished in the corresponding Xe (5p) photoemission spectrum excited with HeI-radiation (see Figure 11 a-d). Both dominant emission peaks, Xe ($5p_{3/2}$) and Xe ($5p_{1/2}$), actually consist of a superposition of up to three peaks. This is clearly seen with the $5p_{1/2}$ signal of the highest spectrum which corresponds to a complete Xe monolayer over the whole 0.05 ML K/Ru (001) surface[40]. The assignment of the three corresponding Xe-states as given

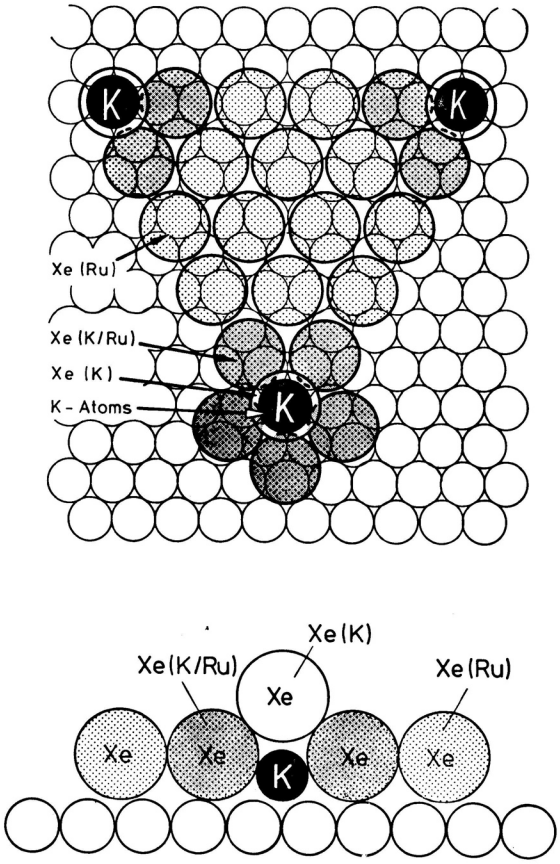

Figure 10. Structure model of a Xe covered 0.05ML K/Ru(001) surface. The small white atoms represent the Ru(001) plane (Ru has hcp structure). Note that at this K-coverage 4 Xe atoms (dotted atoms) may be accommodated between two nearest K-atoms (black atoms); 5 Xe atoms fit round one K-atom and 1 Xe atom (large white atoms) on top of one K-atom. These three Xe states are denoted Xe(Ru), Xe(K/Ru) and Xe(K), respectively.

in Figure 11a has been discussed in detail elsewhere[41,42] and can be supported as follows. The Xe (Ru) peak is most intense and has an electron binding energy very close to that found on pure Ru (001). The Xe (K) peak is smallest, it is shifted most from the Xe (Ru) peak position and it appears only near monolayer completion (because the adsorption energy of Xe on potassium is much smaller than on Ru). The Xe (K/Ru)-state populates first (because the sites next to a K-atom on Ru (001) provide the highest coordination for the physisorbed Xe probe atoms) and has an electron binding energy between those of the Xe (Ru) — and the Xe (K)-states. A quantitative decomposition of the Xe monolayer spectrum from Figure 11a (using sets of three Lorentzians per Xe state as shown in Figure 3) into the three contributions is shown in Figure 12a. The three vertical arrows mark the energy positions E_B^F of the

three Xe ($5p_{1/2}$) signals, from which the local work function φ_{loc} have been calculated using equ. (3) (see Figure 12a). The percentages denote the relative intensity of each Xe-state. Note that the Xe (K/Ru)-state is five times more intense than the Xe (K)-state in excellent agreement with the expectation based on the structure model in Figure 10.

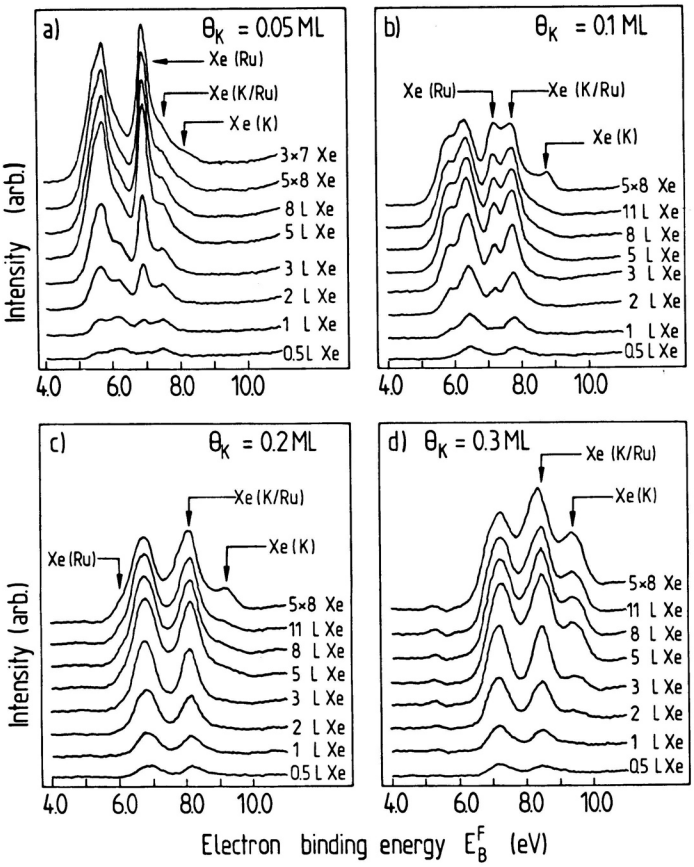

Figure 11. Xe ($5p_{3/2,1/2}$) photoemission spectra for different Xe coverages on four Ru(001) surfaces covered with 0.05 ML, 0.1 ML, 0.2 ML and 0.3 ML potassium, respectively. In each panel the highest spectrum corresponds to a saturated Xe monolayer on the respective surface. Note the successive growth of up to three Xe states as the Xe coverage increases, as can be seen most clearly from the $5p_{1/2}$ emission which in the four panels occurs at electron binding energies E_B^F greater than a) 6.7 eV, b) 7.0 eV, c) 7.5 eV and d) 7.9 eV. In panel c) Xe(Ru) points to the $5p_{3/2}$ component of the corresponding emission. (From Ref. 52)

A decomposition of the PAX-monolayer spectrum from the 0.1 ML K/Ru (001) surface (Figure 11b) is shown in Figure 12b. Again the intensity ratio between the Xe (K/Ru) and the Xe (K) state is 5 as expected, but the electron

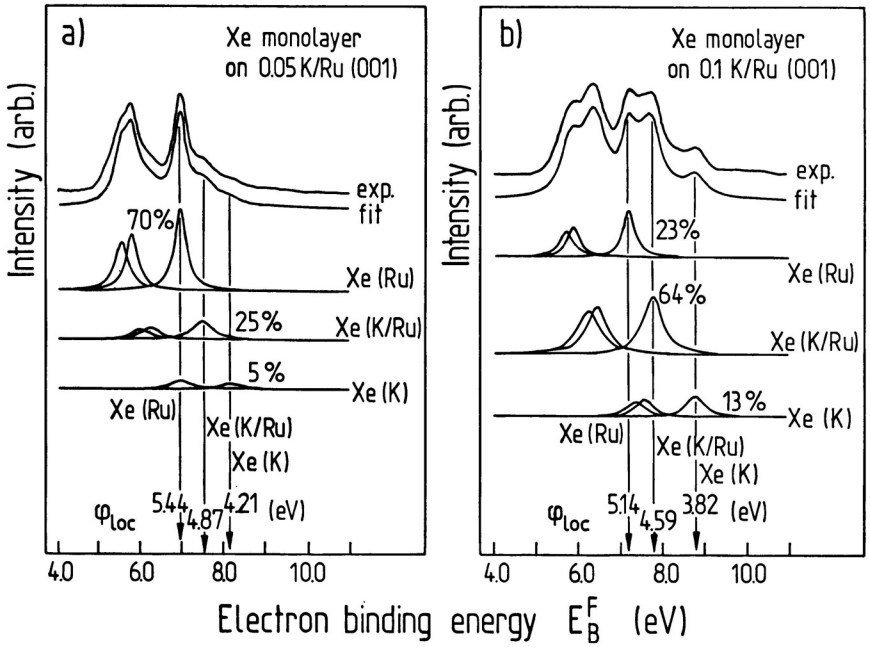

Figure 12. Decomposition of the Xe monolayer PAX spectra from a) the 0.05 ML K/Ru(001) and B) the 0.1 ML K/Ru(001) surface into the three component spectra arising from Xe atmos on free Ru(001) sites [Xe(Ru)], next to K-atoms [Xe(K/Ru)] and on top of K-atoms [Xe(K)]. The percentages give their relative intensities; the φ_{loc}-values are calculated using equs. (2) and (3) and correspond to the local work function at the respective adsorption site. (From Ref. 52)

binding energies of all three Xe states and, hence, the corresponding local work functions are slightly changed with respect to those from the 0.05 ML K/Ru (001) surface. This trend continues for $\Theta_K > 0.1$ ML (Figures 11c and d), and also the intensity ratio of the Xe (K/Ru) and Xe (K) states is no longer near five. Both deviations are easy to conceive in terms of the average distance between two K-atoms on the surface at different coverages. At $\Theta_K = 0.05$ ML this interatomic distance permits to place 4 Xe atoms between two K-atoms (see Figure 10), two of which are Xe (K/Ru)-atoms, while the other two are Xe (Ru)-atoms. Obviously these latter two experience a local work function which is hardly changed (80 meV), from that of a K-free Ru (001) surface. At coverages $\Theta_K > 0.05$ ML, the spheres of electronic perturbation around the individual K-atoms begin to overlap thereby causing a shift of the whole PAX-spectrum including the Xe (Ru) state (Figure 12b). From this we must conclude that the range of electronic perturbation is mainly confined to within a radius of $r \approx 8$ Å around a K-atom, namely $1/2\, r_K + 3/2\, r_{Xe}$; this is rather short ranged. For coverages $\Theta_K \geq 0.5$ ML Xe (K/Ru)-atoms begin to belong to two K-atoms simultaneously. As a consequence the intensity ratio I(Xe(K(Ru))/I(Xe(K)) decreases below 5.

The strongly localized work function decrease measured with the 0.05 ML K/Ru (001) surface next to a K-atom (by means of Xe (K/Ru) ($5p_{1/2}$)) and ontop of a K-atom (by means of Xe (K) ($5p_{1/2}$)) are in excellent agreement with theoretical predictions by Lang and coworkers.[13,44] At the respective locations of the centers of Xe (K/Ru)- and Xe (K)-atoms they predict local surface potential decreases of $\varphi_{loc(K/Ru)} = -550$ meV and $\varphi_{loc(K)} = -1300$ meV, respectively. The corresponding experimental values are —570 meV and —1230 meV as calculated from Figure 12a.

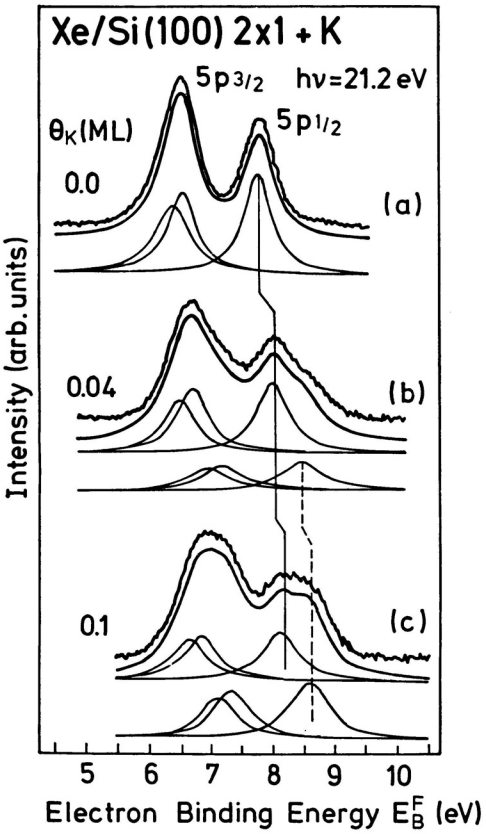

Figure 13. Xe ($5p_{3/2,1/2}$) spectra from an n-Si (100) 2 × 1 surface covered with a) no, b) 0.04 ML and c) 0.1 ML potassium. The quantitative decomposition of the PAX spectra yields one Xe adsorption state on the clean Si (100) 2 × 1 surface [Xe(Si)] and two Xe states [Xe(Si), Xe(K/Si)] on the two other surfaces. (Under the chosen experimental conditions Xe does not adsorb on top of potassium). (From Ref. 52)

A rather similar behavior is observed for K-adsorption on a semiconductor surface, namely Si (100) 2 × 1 as illustrated in Figure 13. But while on the 0.05 ML K/Ru (001) surface the Xe (Ru) state was hardly shifted (~ 80 meV) from the position found on bare Ru (001), on the 0.04 ML K/Si (100) 2 × 1 surface the Xe (Si) is shifted by ~ 400 meV compared to the clean Si (100)

2 × 1 surface. This seems to be in accord with the different screening lengths typical for metals versus semiconductors.

5. GROWTH AND STABILITY ON TWODIMENSIONAL ALLOY BILAYERS

The thermal stability of metal-metal interfaces is of great importance for the design and the application of layered structures. The thermal degradation of layered materials starts with the exchange of atoms across the interface. This process, which cannot easily be followed in buried interfaces, can be studied in model systems consisting of evaporated (sub)monolayers of one metal on top of another. In this section we use photoemission of adsorbed

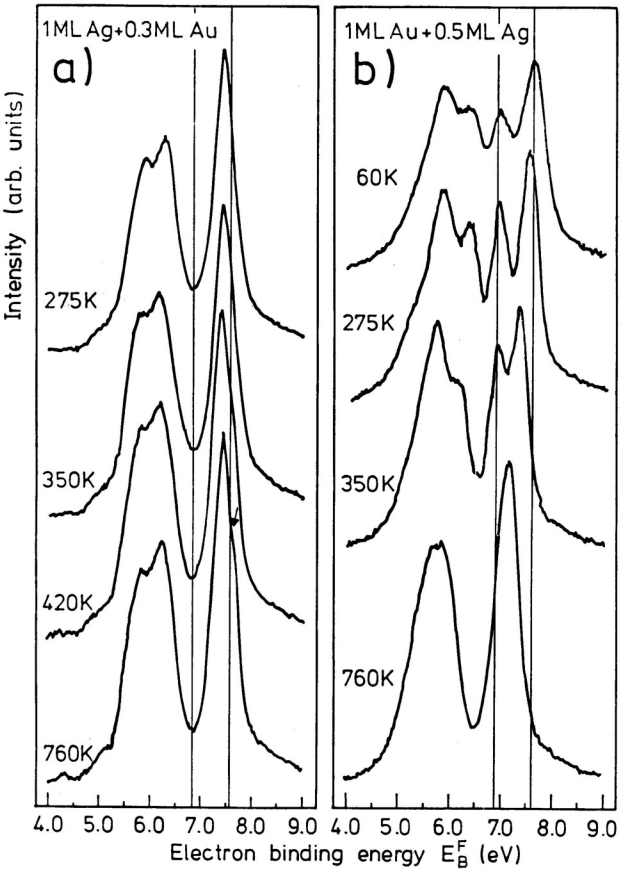

Figure 14. Photoemission spectra of Xe $5p_{3/2,1/2}$ electrons (PAX spectra) from a monolayer of Xe adsorbed at 60 K on Au/Ag and Ag/Au double layers, consisting of (a) a complete monolayer of Ag on Ru(001) covered with 0.5 ML of Au and (b) a complete monolayer of Au covered with 0.5 ML of Ag. The samples have been annealed at the indicated temperatures for 10 min. The vertical lines mark the Xe $5p_{1/2}$ binding energies of Xe on Au (6.8 eV) and Xe on Ag (7.6 eV). The spectral changes in the Xe signals reflect the thermally activated redistribution of Ag and Au at the surface.

xenon in order to investigate the thermally activated exchange of atoms across the atomically sharp interface between Au and Ag layers of monoatomic thickness, prepared by evaporation onto a Ru (001) substrate. Both Ag and Au form a compressed, (111)-like monolayer on Ru (001)[45] and do not penetrate into the Ru crystal like Cu.

5.1 *Silver/Gold Bilayer on Ru(001)*

Figure 14. shows the PAX monolayer spectra of a layer structure consisting of a well-annealed monolayer of Au on Ru (001), with the equivalent of 0.5 monolayer (ML) Ag on top. The latter has been deposited at 60 K. The spectrum clearly shows two distinct peaks, namely, of Xe adsorbed on Ag and of Xe on Au. In addition, significant intensity is seen at positions between the Xe/Au and Xe/Ag peaks, where contributions from Xe on Ag-Au mixed sites are expected. Clear evidence for the existence of these sites is obtained from PAX spectra taken at different Xe coverages, which are shown in Figure 15.

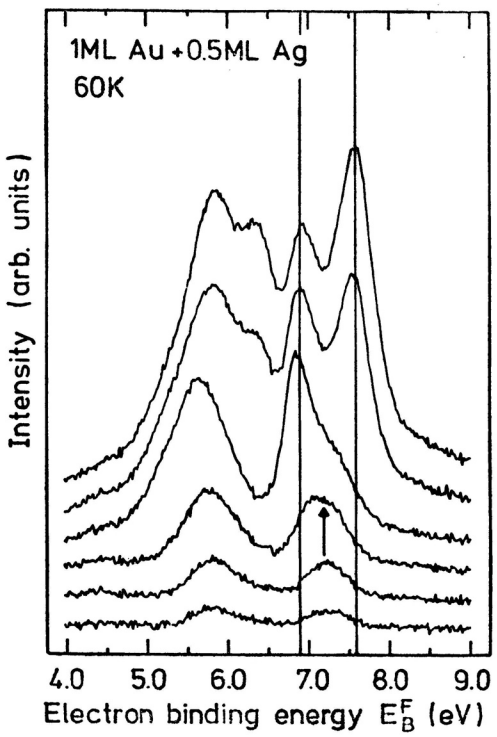

Figure 15. PAX spectra for different coverages of Xe adsorbed at 60 K on the annealed 0.5 ML Ag/1ML Au/Ru(001) system. The spectra show how the different sites are populated by Xe in the order of increasing adsorption energy. At low exposures, Xe is adsorbed exclusively on mixed Ag-Au sites. Next, at intermediate Xe exposures, the Au sites are populated (6.8 eV) and finally, the Ag sites (7.6 eV). The top spectrum corresponds to a Xe monolayer and is the same as the top spectrum of Figure 14b.

Figure 15. illustrates how the different sites on the surface are populated by xenon in the order of decreasing absorption energy. The spectra obtained after low Xe exposures (lower traces in Figure 15) exhibit a broad Xe ($5p_{1/2}$) peak in the region between 7.0 and 7.3 eV (see arrow). At intermediate exposure, the Au sites (peak at 6.8 eV) are populated, and finally the Ag sites (7.6 eV). With respect to the nature of the mixed sites it is important to mention that the Ag-Au sites on a flat alloy are populated after Xe has filled all available Au sites.[46] We therefore consider the sequence of site population in Figure 15 as evidence that the mixed sites are sites of high coordination, such as those adjacent to adatoms and steps of Ag on Au, where Xe is bound more strongly than on flat sites.

We interpret the results of Figure 15 as follows: The evaporated Ag atoms which arrive at the Au/Ru (001) surface held at 60 K stay at the site of impact and form a highly disordered Ag overlayer on the Au monolayer. When the sample is heated to 275 K for 10 min and subsequently cooled down to 60 K, the PAX monolayer spectrum labelled 275 K in Figure 14b is measured. It still shows the peaks of Xe on Au and Xe on Ag, but the intensity of Xe on the mixed Ag-Au sites has decreased significantly. Curve fitting indicates that the intensities of both Xe (Ag) and Xe (Au) increased with respect to the spectrum of the unannealed sample. The increase of the Xe (Ag) intensity most probably implies that the initial sample contained three-dimensional clusters of Ag, which were destroyed by annealing at 275 K. In spite of the fact that more Au atoms are now covered by Ag, the Xe (Au) intensity increased also, at the expense of the mixed Ag-Au sites of high coordination. The results suggest that upon heating to 275 K the initially disordered, defect overlayer of Ag atoms and clusters is transformed to Ag islands, on top of the Au monolayer on Ru (001). This structure forms the model system for an atomically sharp interface between Ag and Au.

Annealing at 350 K and subsequent cooling to 60 K gives the third spectrum of Figure 14b. Note that the Xe (Ag) peak is no longer present. The spectrum shows in addition to the Xe (Au) peak a new, relatively narrow peak at —7.3 eV, which is again characteristic of Xe on mixed Ag-Au sites. However, a series of PAX spectra of different Xe coverages[46] shows that these mixed sites are populated after the Au sites, suggesting that the mixed sites are present as »flat« islands of Ag-Au alloy. Curve fitting of this spectrum yields that the Au intensity is about the same as in the previous situation of Ag islands on Au. Hence, we conclude that after annealing of Ag islands on a Au monolayer at 350 K, Ag atoms which were initially on Au, and Au atoms which were initially covered by Ag islands, have exchanged to form a Ag-Au alloy. The uncovered Au, however, has not been affected.

The bottom spectrum in Figure 14b has been measured after the sample has been annealed at 760 K. The peak of Xe on Au is absent now and almost all intensity is in the range between 7.0 and 7.3 eV, implying that all Au and Ag on the Ru (001) surface have mixed to form an alloy. Note that the peak of Xe on AgAu has shifted to a lower binding energy in comparison to the previous spectrum, which is in agreement with the fact that a homogeneous alloy formed from 1-ML Au and 0.5-ML Ag contains more Au than the approximately 50% Ag-50% Au alloy islands of the sample annealed at 350 K.

Hence, the results in Figure 14b show that the double layer containing the atomically sharp interface between Ag and Au on Ru (001) is stable at temperatures up to about room temperature. Exchange between Ag and Au atoms is detectable already at 350 K.

5.2 *Gold/Silver Bilayer on Ru(001)*

We now turn to a series of experiments in which Ag was deposited first as a complete monolayer, and subsequently Au. The amount of Au deposited at 60 K is the equivalent of 0.3 ML. Figure 14a shows the PAX monolayer spectra for this Au/Ag/Ru (001) sample. The top spectrum corresponds to the system after annealing at 275 K and recooling to 60 K. It consists of a broad peak in the range between 7.2 and 7.7 eV, characteristic of Xe on Ag-Au mixed sites and on pure Ag sites. Note that the spectrum contains no contribution from Xe on Au, which proves that although Au was deposited on the Ag monolayer, no pure Au patches have been formed. This suggests that at 275 K Au has already started to penetrate into the Ag underlayer, and that the Au in the second layer has Ag neighbors; otherwise at least some intensity of Xe on Au should have been observed. The relatively high intensity of Xe on Ag-Au sites with respect to Xe on Ag suggests that Au has not agglomerated into islands before it started to exchange with the underlayer.

Further annealing of the system at 350 and 420 K causes only minor changes of the resultant PAX spectra. The spectrum measured after annealing at 760 K, however, exhibits a wellresolved shoulder near the binding energy of Xe on pure Ag (see arrow in Figure 14a). In addition, the spectrum of the Ag-Au mixed sites has sharpened up, indicating that the alloy has a more homogeneous composition. A quantitative decomposition of the spectra[46], as well as the order in which the sites are populated, and the way in which the splitting of the Xe $5p_{3/2}$ peaks develops with increasing Xe coverage, all support the interpretation that the sample annealed at 760 K consists of a monolayer of Ag-Au alloy, with Ag islands on top.

5.3 DISCUSSION

The results presented in the two previous sections are summarized in Figure 16. They show that the Ag/Au interface in the Ag/Au/Ru (001) layer structure is thermally more stable than the Au/Ag interface in the Au/Ag/Ru (001) system. In the former Ag does not penetrate the Au underlayer below 275 K, and the final equilibrium state after annealing at 760 K is a more or less homogeneous alloy in two layers. In contrast to this, Au atoms deposited initially on the Ag underlayer at 60 K, exchange site with the underlying Ag atoms already at 275 K. After equilibration at 760 K, this system consists of a 70% Ag—30% Au alloy monolayer, covered in part by submonolayer Ag islands. These conclusions on the equilibrated systems are in good agreement with earlier thermal desorption spectra on bi-layer Ag-Au alloys[47]. Among the factors which determine the remarkable difference in thermal stability between the Ag/Au/Ru (001) and the Au/Ag/Ru (001) layer structures are the following: (a) The bond between isolated Au atoms and the Ru (001) is $\sim$ 390 kJ/mol and is almost 150 kJ/mol stronger than the 245 kJ/mol bet-

ween Ag and Ru (001)[48]. (b) The surface free energy of Ag (1140 erg/cm^2) is lower than that of Au (1400 erg/cm^2)[49]. (c) The lateral interaction energy between Ag on Ru (001) is attractive[48]. (d) The heat of formation of Ag-Au alloys is slight exothermic[50].

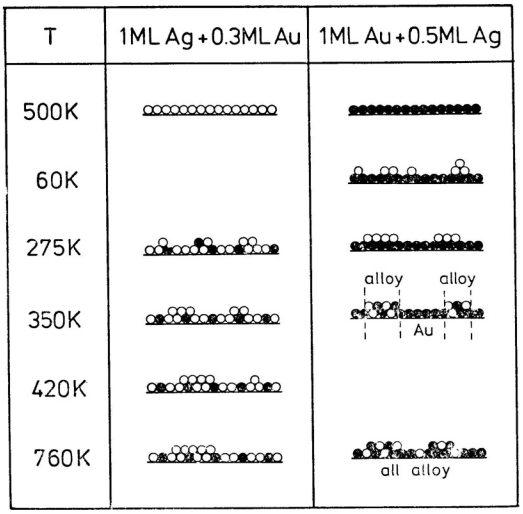

Figure 16. Illustration of the structural changes in Au/Ag and Ag/Au double layers caused by annealing, as suggested by the PAX spectra in Figure 14.
○ Ag atoms; • Au atoms.

The first two terms favor Au atoms to get in contact with the Ru (001) substrate. This process, however, will compete with the exothermicity of the AuAu alloy formation which tends to maximize the number of Ag-Au-bonds. The attractive Ag-Ag interaction explains the formation of Ag islands in the case where Ag has segregated to the second layer.

This example of the double layers on Ru (001) illustrates that certain properties of interfaces, such as their thermal stability, can be studied in model systems consisting of consecutively deposited monolayers, and that again PAX appears as a very sensitive tool in characterizing the surfaces of these layer structures on an atomic scale.

6. SUMMARY AND CONCLUSIONS

As demonstrated in this review it is possible to determine local work functions by means of PAX with a lateral »resolution« of 5—10 Å. Whenever available, theroretical predictions are in excellent agreement with the experimental findings. As a result detailed information can be obtained about the concentration and distribution of structural and chemical defects at metal surfaces as well as about their local surface potential on an atomic scale. The presented examples include the characterization of surface steps; of submonolayer films of adsorbed potassium on both a metal and a semiconductor surface, and the growth and thermal stability of evaporated metal and alloy films. In most of these cases the substrate was a Ru (001) surface, because

the adsorbed metals could be completely desorbed again in order to restore the clean substrate. The selected examples are case studies, which are to show the capability and the methodical procedure of PAX measurements. But it is obvious, that similar experiments will provide invaluable microscopic information about other structurally and chemically heterogeneous surfaces likewise. It is also believed that the verification of strong local surface potential variations and, hence, the existence of strong localized fields arising hereof is relevant for an understanding of processes at both solid/gas and solid/liquid interfaces.

Finally, comparing PAX with Scanning Tunneling Microscopy (STM) it appears that to some extend both techniques provide complementary information. STM reliefs provide a real image of the atomic topography of a surface. At metal surfaces the spatial resolution is 3—5 Å laterally (x, y) and 0.1 Å vertically (z). Because of this high resolution the STM is uniquely suited to characterize the location and the geometry of individual defects. But also because of its very high resolution the STM should not be utilized to scan large surface areas in order to determine defect densities. This information may be easier obtained by means of PAX. The partial PAX (Xe $5p_{1/2}$) intensities are a direct measure of the relative surface concentrations of specific kinds of surface sites, e. g. structural defects or hetero-atoms. In many respects it is more important to know the number of certain defects than their exact location, for example when evaluating the reactivity and catalytic activity of a surface. This argument may be extended to the characterization of powder samples, where the application of the STM does not seem to be of obvious help. In turn, PAX studies of a bimetallic Cu/Ru powder catalyst have provided interesting information about purity and surface roughness of the particles[32]

REFERENCES

1. C. T. Campbell, G. Ertl, H. Kuipers, J. Segner, *Surface Sci.* **107** (1980) 412.
2. H. Shimizu, K. Christmann, G. Ertl, *J. Catalysis* **61** (1980) 412.
3. a) H. P. Bonzel, *J. Vac. Sci. Technol.* **A2** (1984) 866.
   b) G. Ertl in: *Catalysis, Science and Technology*, Vol. **4**, Eds. J. R. Anderson and M. Boudart (Springer Verlag, Berlin, 1983) p. 209.
4. a) P. Soukiassian, M. H. Bakshi, Z. Hurych, *J. Appl. Phys.* **61** (1987) 2679.
   b) P. Soukiassian, M. H. Bakshi, H. I. Starnberg, A. S. Bommannavar, Z. Hurych, *Phys. Rev.* **B38** (1988) 6496.
5. a) G. A. Somorjai, *Chemistry in Two Dimensions: Surfaces.* Ithaca: Cornell University Press 1981.
   b) B. Lang, R. W. Joyner, G. A. Somorjai, *Surface Sci.* **30** (1972) 440.
   c) D. W. Blakely, G. A. Somorjai, *Surface Sci.* **65** (1977) 419.
6. a) G. Binnig, H. Rohrer, *Surface Sci.* **127** (1983) 236; *Surface Sci.* **152/153** (1985) 17.
   b) R. J. Behm, W. Hösler, in: *Physics and Chemistry of Solid Surfaces* VI, Ed. R. Vanselow, R. Howe (Springer, Berlin, Heidelberg 1986).
7. W. Tielips, E. Bauer, *Surface Sci.* **162** (1985) 163; see also *Ultramicroscopy* **17** (1985) 51, 57.
8. a) K. Wandelt, *J. Vac. Sci. Technol.* **A2** (1984) 802.
   b) K. Wandelt in: *Studies in Surface Science and Catalysis*, Eds. B. Delmont, J. T. Yates, Vol. **32** *Thin Metal Films and Gas Chemisorption*, Ed. P. Wissmann (Elsevier, Amsterdam, 1987) p. 280—368.
9. B. J. Waclwaski, J. F. Herbst, *Phys. Rev. Lett.* **35** (1975) 1594.

10. R. P. Antoniewicz, *Phys. Rev. Lett.* **38** (1977) 374.
11. S. I. Ishii, Y. Ohno, *J. Electron Spectrosc.* **33** (1984) 85.
12. K. Horn, M. Scheffler, A. M. Bradshaw, *Phys. Rev. Lett.* **44** (1978) 822.
13. M. Scheffler, K. Horn, A. M. Bradshaw, K. Kambe, *Surf. Sci.* **80** (1979) 69.
14. K. Wandelt, *J. Vac. Sci. Technol.* **A2** (1984) 802.
15. J. Hulse, J. Küppers, K. Wandelt, G. Ertl, *Appl. Surf. Sci.* **6** (1980) 453.
16. K. Wandelt, J. W. Niemantsverdriet, P. Dolle, K. Markert, *Surf. Sci.* **213** (1989) 612.
17. N. D. Lang, A. R. Williams, *Phys. Rev.* **B25** (1982) 2940.
18. J. Behm, C. R. Brundle, K. Wandelt, *J. Chem. Phys.* **85** (1986) 1061.
19. A. Jablonski, S. Eder, K. Wandelt, *Appl. Surf. Sci.* **22/23** (1985) 309.
20. H. Wagner, in: *Springer Tracts in Modern Physics,* Vol. **85** (Springer, Berlin, Heidelberg, 1979).
21. R. J. Behm, W. Hösler,, E. Ritter, G. Binnig, *Phys. Rev. Lett.* **56** (1986) 228.
22. R. Miranda, S. Daiser, K. Wandelt, G. Ertl, *Surf. Sci.* **131** (1983) 61.
23. K. Wandelt, J. Hulse, *J. Chem. Phys.* **80** (1984) 1340.
24. S. Daiser, *Diplom-Thesis,* University of München, 1981.
25. K. Wandelt, in: *Chemistry and Physics of Solid Surfaces* VIII, Eds. R. Vanselow, and R. Howe, Springer Series in Surface Science (Springer, Berlin, Heidelberg) in press.
26. R. Smoluchowski, *Phys. Rev.* **60** (1941) 661.
27. K. Besocke, H. Wagner, *Surf. Sci.* **52** (1975) 653.
28. K. Besocke, H. Wagner, *Phys. Rev.* **B8** (1973) 4597.
29. S. Daiser, K. Wandelt, *Surf. Sci.* **128** (1983) L213.
30. B. Gumhalter, K. Hermann, K. Wandelt, *Vacuum,* in press; see also in: B. Gumhalter, M. Milun, K. Wandelt, *Selected Studies of Adsorption on Metal and Semiconductor Surfaces,* Scientific Series of the International Bureau (KFA-Jülich GmbH, 1989).
31. S. Eder, K. Markert, A. Jablonski, K. Wandelt, *Ber, Bunsengesell. Phys. Chem.* **90** (1986) 225.
32. K. S. Kim, J. H. Sinfelt, S. Eder, K. Markert, K. Wandelt, *J. Phys. Chem.* **91** (1987) 2337.
33. K. Christmann, G. Ertl, H. Shimizu, *Thin Solid Films,* **57** (1979) 247, and *J. Catalysis* **61** (1980) 397.
34. M. Kiskinova, G. Pirug, H. P. Bonzel, *Surf. Sci.* **133** (1983) 321.
35. E. M. Oellig, R. Miranda, *Surf. Sci.* **177** (186) L947.
36. G. Surnev, *Surf. Sci.* **110** (1981) 45.
37. I. Langmuir, *J. Amer. Chem. Soc.* **54** (1932) 2798.
38. I. Langmuir, J. B. Taylor, *Phys. Rev.* **40** (1932) 463.
39. J. B. Taylor, I. Langmuir, *Phys. Rev.* **B44** (1933) 423.
40. The Completion of the first Xe monolayer is best verified by means of thermal desorption as well as photo-emission experiments. The desorption temperature of 2. layer Xe atoms is significantly lower than that of 1. layer Xe atoms. The photoemission peaks from 2. layer Xe atoms are shifted to higher E_B^F-values with respect to those from the 1. layer.
41. K. Markert, *Diplom-Thesis,* University of München, 1985.
42. K. Markert, K. Wandelt, *Surf. Sci.* **159** (1985) 24.
43. J. K. Norskov, S. Holloway, and N. D. Lang, *Surf. Sci.* **137** (1984) 65.
44. N. D. Lang, S. Holloway, and J. K. Norskov, *Surf. Sci.* **150** (1985) 24.
45. B. Konrad, F. J. Himpsel, W. Steinmann, K. Wandelt, in: *Proceedings of the ER-LEED 85 Meeting,* Erlangen, FRG, 1985, p. 109.
46. K. Wandelt, J. W. Niemantsverdriet, P. Dolle, K. Markert, *Surf. Sci.* **213** (1989) 1752.
47. K. Markert, P. Dolle, J. W. Niemantsverdriet, K. Wandelt, *J. Vac. Sci. Technol.* **A6** (1988) 1752.
48. J. W. Niemantsverdriet, P. Dolle, K. Markert, K. Wandelt, *J. Vac. Sci. Technol.* **A5** (1987) 875.

49. G. A. Somorjai, *Chemistry in Two Dimensions: Surfaces* (Cornell University, Ithaca, 1981), p. 31.
50. P. Hultgren, R. L. Orv, P. D. Anderson, K. K. Kelley in: *Selected Values of Thermodynamic Properties of Metals and Alloys* (Wiley, New York, 1963), p. 341.
51. K. Wandelt, in: *Lectures on Surface Science*, Eds. G. R. Castro, M. Cardona (Springer Verlag, Berlin, Heidelberg, 1987), p. 273.
52. K. Wandelt, in: *Physics and Chemistry of Alkali Metal Adsorption*, Eds. H. P. Bonzel, A. M. Bradshaw, G. Ertl (Elsevier, Amsterdam, 1989), p. 25.

SAŽETAK

Neuređene čvrste površine: karakterizacija i svojstva

Klaus Wandelt

Neuređenost površina na dimenziji atoma (površinski defekti) ima značajan, vjerojatno i prevladavajući utjecaj na fizička i kemijska svojstva čvrstih površina, i to na reaktivnost i katalitička svojstva. Upravo je stoga potrebno raspolagati istraživačkim tehnikama, koje su u stanju ukazati na strukturu na atomskoj skali. Zahtjevi te naravi doveli su do razvoja eksperimentalnih tehnika od kojih su neke opisane u ovom radu. Jedna od njih je fotoemisija iz adsorbiranog ksenona (PAX) pod uvjetima ultravisokog vakuuma. Pomoću te tehnike moguće je odrediti lokalnu radnu funkciju (work function) uz lateralnu rezoluciju od 0,5 do 1 nm. U većini opisanih eksperimenata supstrat je bila površina Ru(001) stoga što je sa takve dobro definirane površine moguće desorpcijom ukloniti adsorbat i povratiti je u početno stanje. Opisane eksperimente i metodologiju treba shvatiti kao primjere, koji ukazuju na mogućnosti i domete metode. Usporedbom sa skanerskim tunelirajućim mikroskopom (STM *Scanning Tunneling Microscope*) proizlazi da se obje tehnike međusobno nadopunjuju, s time da je kod STM-a prostorna rezolucija 0,3 do 0,5 nm, a vertikalna do 0,01 nm, ali je nepodesna za proučavanje površina disperznih materijala. Dobivene informacije o relativnim koncentracijama kemijskih i strukturnih defekata jednako su važne za razumijevanje svojstava granice faza čvrsto/plin, kao i one čvrsto/tekuće.